INVESTIGATION OF THE EFFECT OF ANNEALING ON IRRADIATED ALLOY 718

A Thesis

by

HALEY BROOKE TURMAN

Submitted to the Office of Graduate and Professional Studies of
Texas A&M University
in partial fulfillment of the requirements for the degree of

MASTER OF SCIENCE

Chair of Committee,	Matt Pharr
Committee Members,	Lin Shao
	Alan Freed
Head of Department,	Andreas A. Polycarpou

May 2019

Major Subject: Mechanical Engineering

ABSTRACT

During normal accelerator operations at the Isotope Production Facility (IPF) within the Los Alamos Neutron Science Center (LANSCE) at Los Alamos National Laboratory (LANL), an annealed Alloy 718 proton beam window experiences a peak temperature of 120°C but can have up to 100°C fluctuations due to nonstandard runs. These fluctuations can anneal radiation damage and possibly cause precipitation of other phases. To this end, this study aimed to systematically determine the effects of deliberate temperature excursions on the microstructure and mechanical properties of irradiated Alloy 718. We characterized properties of a set of Alloy 718 samples irradiated to 15 dpa under three temperatures (room temperature, 100°C, and 200°C) and subsequently annealed at three conditions (none, 300°C, and 500°C). Additionally, we characterized samples irradiated to 0.5 dpa at 100°C and annealed under three conditions (room temperature, 100°C, and 200°C). Each condition was compared quantitatively and qualitatively with unirradiated annealed Alloy 718. Microstructural evolution, including determining the presence and prevalence of precipitates and dislocations was carried out with a Transmission Electron Microscope (TEM). Additionally, nanoindentation testing was completed on the samples to determine the influence of these treatments on mechanical properties. The study has shown via TEM that precipitates do not form under any of the investigated conditions. However, a strong trend of decreasing hardness with increasing annealing temperature was observed across all samples. In other words, annealing does indeed change the specimen back toward its initial state prior to irradiation.

Although further testing is necessary to provide certainty, we attribute this trend to a decrease in dislocation density in the samples during annealing, as observed through TEM analysis. Overall, these results indicate that in-situ annealing radiation damage from the IPF window is indeed feasible.

DEDICATION

I would like to dedicate this work to my parents, who devoted their time, energy, and effort so that I could excel. Without their support and encouragement, I would not be where I am today.

ACKNOWLEDGEMENTS

I would like to thank my advisor, Dr. Matt Pharr, for his support and guidance throughout my research and graduate education. I would also like to thank Dr. Alan Freed and Dr. Lin Shao for serving as my committee members.

My thanks also go to Mike Borden and Keith Woloshun at Los Alamos National Laboratory for their guidance. They supported and advocated for my work, which enabled me pursue research on a project I enjoyed. I would also like to thank Stu Maloy for his invaluable technical guidance and support as I gained knowledge of my research area. I also thank Jonathan Gigax at LANL for his support.

Additionally I would like to thank my colleagues at Texas A&M, Cole Fincher and Hyosim Kim, as well as Hi Vo at UC Berkeley, who provided much appreciated advice and guidance. I am immensely grateful for the support they provided.

I would like to thank Eda Aydogan at LANL and Aaron French at the Radiation Materials Science Laboratory and Characterization Facility at Texas A&M University for their work in electropolishing the samples and irradiating the 15 dpa set, respectively. Finally, my thanks go to Matthew Chancey at LANL for his tireless work in irradiating the 0.5 dpa samples.

CONTRIBUTORS AND FUNDING SOURCES

This work was supervised by a thesis committee consisting of Professors Matt Pharr (advisor) and Alan Freed of the Department of Mechanical Engineering and Professor Lin Shao of the Department of Nuclear Engineering. Additionally, Stuart Maloy and Keith Woloshun of Los Alamos National Laboratory served as outside advisors for this work.

The 15 dpa samples were electropolished by Eda Aydogan at Los Alamos National Lab. The 15 dpa irradiations were carried out at the Radiation Material Science Laboratory and Characterization Facility at Texas A&M University by Aaron French. The 0.5 dpa irradiations were completed at Los Alamos National Lab, as organized by Jonathan Gigax and Stuart Maloy.

Graduate study and research was primarily funded by the Isotope Production Facility at Los Alamos National Laboratory (subcontract #477029). The study was also partially funded by Matt Pharr's startup funds from Texas A&M University, the Department of Mechanical Engineering at Texas A&M University, as well as the Texas A&M University Engineering Experiment Station.

NOMENCLATURE

α	Dislocation strength constant
α_{loops}	Dislocation strength constant related to loops
$\alpha_{precipitates}$	Dislocation strength constant related to loops
b	Burgers vector magnitude
β	Work hardenability measure
CSM	Continuous stiffness measurement
d	Diameter of dislocation
d_{grain}	Diameter of grain
d_{loop}	Diameter of loop
dpa	Displacement per atom
ε	Strain
FIB	Focused Ion Beam
H	Hardness
IPF	Isotope Production Facility
k	Constraint factor
LANL	Los Alamos National Laboratory
LANSCE	Los Alamos Neutron Science Center
M	Taylor factor
MCNPX	Monte Carlo N-Particle Transport Code eXtended
μ	Shear modulus

N	Number of dislocation per unit volume
PH	Precipitation Hardened
PKA	Primary knock-on atom
ρ_d	Dislocation density
σ_F	Friction stress
σ_{loops}	Stress due to loops
σ_{LR}	Long range stress
$\sigma_{precipitates}$	Stress due to precipitates
σ_{SR}	Short range stress
σ_y	Yield stress
TEM	Transmission Electron Microscope

TABLE OF CONTENTS

Page

ABSTRACT ii

DEDICATION iv

ACKNOWLEDGEMENTS v

CONTRIBUTORS AND FUNDING SOURCES vi

NOMENCLATURE vii

TABLE OF CONTENTS ix

LIST OF FIGURES xi

LIST OF TABLES xiii

CHAPTER I INTRODUCTION AND LITERATURE REVIEW 1

1.1 Introduction 1
1.2 Isotope Production Facility 2
1.3 Previous Isotope Production Facility Window Testing 5
1.4 Alloy 718 Properties and Microstructure 6
1.5 Overview of the Effect of Irradiation on Metals 7
1.6 Review of Studies on Irradiated Alloy 718 10
1.6.1 Irradiated Alloy 718 Mechanical Properties 10
1.6.2 TEM Analysis of Irradiated Alloy 718 in the Annealed and PH Conditions 12

CHAPTER II RESEARCH OBJECTIVES AND SAMPLE PREPARATION 14

CHAPTER III NANOINDENTATION RESULTS 19

3.1 Nanoindentation Results – 15 dpa 20
3.2 Nanoindentation Results – 0.5 dpa 28

CHAPTER IV TEM ANALYSIS 32

CHAPTER V FUTURE WORK 39

CHAPTER VI CONCLUSION 41
REFERENCES 43
APPENDIX A COMPOSITION ANALYSIS 47
APPENDIX B NANOINDENTATION PARAMETERS 48
APPENDIX C ADDITIONAL HARDNESS VS. DEPTH CURVES 49

LIST OF FIGURES

Page

Figure 1. LANSCE Schematic [4] 3

Figure 2. Isotope Production Facility Layout [4] 3

Figure 3. The window welded to the end of the pipe (left) and the beam profile on the window outlined in red (right) 4

Figure 4. Dosage Curve and Region of Interest for 15 dpa Nickel Ion Irradiation 16

Figure 5. Dosage Curve and Region of Interest for 0.5 dpa Proton Irradiation 17

Figure 6. Example of Optically Imaged Indent 19

Figure 7. Room Temperature Irradiation Load Depth Curves (15 dpa) 20

Figure 8. 100°C Irradiation Load Depth Curves (15 dpa) 21

Figure 9. 200°C Irradiation Load Depth Curves (15 dpa) 21

Figure 10. Modulus of Elasticity vs. Depth for Room Temperature Irradiations (15 dpa) 23

Figure 11. Modulus of Elasticity vs. Depth Curves for 100°C Irradiations (15 dpa) 23

Figure 12. Modulus of Elasticity vs. Depth Curves for 200°C Irradiations (15 dpa) 24

Figure 13. Hardness vs. Depth Curves for Room Temperature Irradiations (15 dpa) 26

Figure 14. Hardness vs. Depth Curves for 100°C Irradations (15 dpa) 26

Figure 15. Hardness vs. Depth Curves for 200°C Irradations (15 dpa) 27

Figure 16. Hardness vs. Depth Graphs at Varying Irradiation Temperature (15 dpa) 28

Figure 17. Elastic Modulus vs. Depth for 100°C Irradiations (0.5 dpa) 29

Figure 18. Hardness vs. Depth Curves for 100°C Irradiations (0.5 dpa) 31

Figure 19. Example TEM Lamella 33

Figure 20. Precipitate in Room Temperature Irradiation, 500°C Anneal Sample (15 dpa) 34

Figure 21. Chemical Composition of Precipitate and Surrounding Matrix 35

Figure 22. TEM Image of Room Temperature, No Anneal Sample (15 dpa).....36

Figure 23. TEM Image of Room Temperature, 500C Anneal Sample (15 dpa).....36

LIST OF TABLES

Page

Table 1. Allowable Atomic Weight Percent Ranges for Alloy 718 [2] 6

Table 2. 15 DPA Irradiation Parameters 15

Table 3. 0.5-0.67 DPA Irradiation Parameters 15

CHAPTER I

INTRODUCTION AND LITERATURE REVIEW

1.1 Introduction

Alloy 718, sometimes known as Inconel 718, is a high strength nickel-chromium superalloy that is commonly used in the aerospace and nuclear industries due to its high ductility, strength, and corrosion resistance [1-3]. At the Isotope Production Facility (IPF) within Los Alamos National Laboratory (LANL), it is used in a proton accelerator as a beam window. Several factors motivated use of annealed Alloy 718 in this application, including its good ductility, tensile strength, corrosion resistance between room temperature and 500°C, extensive previous use as a window material, good irradiation tolerance up to 20 dpa, and its availability in plate form.

In an accelerator, the beam window allows the beam to pass through to the targets while creating a boundary between high vacuum and ambient air, or high vacuum and a higher pressure area. During normal production runs, the 100 MeV, 250 μA proton beam produces a peak temperature of 120°C, but nonstandard runs can create temperature fluctuations up to 100°C. These fluctuations can possibly anneal radiation damage and possibly cause precipitation of other phases.

The IPF beam window has a finite life due to the mechanical stresses and radiation damage it experiences. It is currently designed for a maximum lifetime of 20 dpa. Practically, this means that every three to five years, IPF must be shut down to remove the

old window and put a new window in its place. This process typically takes several days, thereby producing undesired downtime at the IPF.

Even though it is widely utilized, little research has focused on characterizing the microstructure and mechanical properties of irradiated Alloy 718 as a function of annealing temperature. To this end, this study aims to systematically characterize the evolution of Alloy 718's microstructure and corresponding mechanical properties. Our goal is to determine if annealing of irradiated Alloy 718 can remove enough radiation damage to increase the lifetime of LANL's Alloy 718 windows via in-situ annealing. If possible, in-situ annealing would prevent the loss of productivity associated with frequently replacing the IPF window.

1.2 Isotope Production Facility

Los Alamos National Laboratory in Los Alamos, New Mexico, houses the Los Alamos Neutron Science Center (LANSCE). LANSCE consists of an 800 MeV accelerator with facilities for nuclear weapons research, proton radiography, ultra – cold neutrons, and isotope production. Figure 1 depicts a schematic of LANSCE's layout.

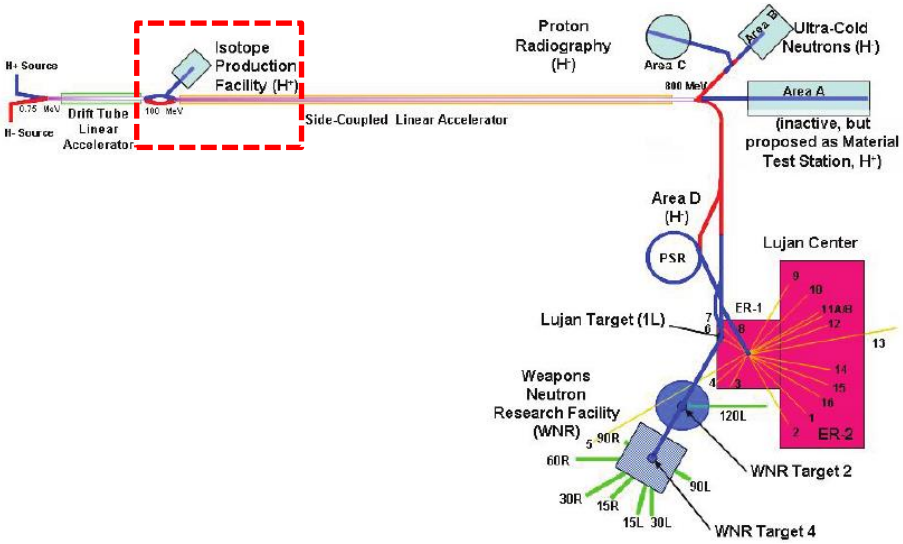

Figure 1. LANSCE Schematic [4]

The Isotope Production Facility (IPF), the location of which is indicated by a red dashed box in Figure 1, utilizes a beam window of Alloy 718. The window serves to isolate the beamline elements, which are under vacuum, from the target, which is held at 17.2 psig due to the 40 ft water column above it. This layout is shown in Figure 2 below.

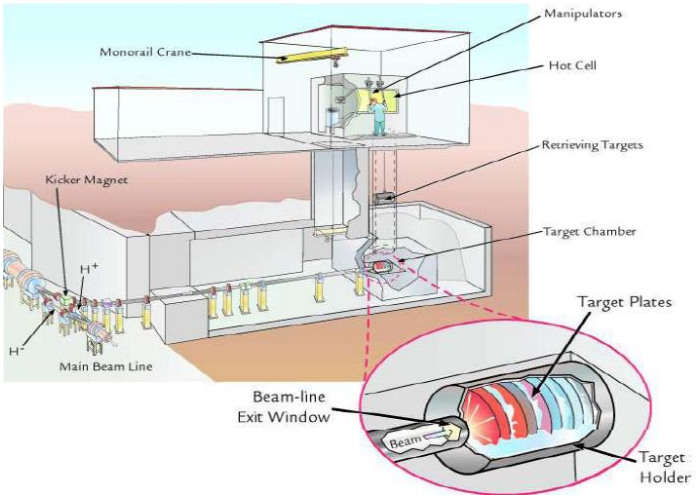

Figure 2. Isotope Production Facility Layout [4]

The 2010 IPF window was 76.2 mm in diameter and 0.635 mm thick. This initially annealed window was in place between May 2004 and December 2009. During this time, the window was subjected to thermal-mechanical stresses caused by volumetric heating and the pressure differential across the surface from the 100 MeV, 250 μA proton beam. The damaged window with burn patterns, which was cut from the beamline, can be seen in Figure 3.

Figure 3. The window welded to the end of the pipe (left) and the beam profile on the window outlined in red (right). Reprinted with permission from [5]

Near the end of a production run, two atypical irradiations occurred at 100 MeV, 355 μA for 1.2 hr and 40 MeV, 250 μA for 1 hr [5]. These irradiations are possible sources for the window's 1.5 mm bulge into the vacuum side as well as the unexpected heating of beamline elements. The collimator, located about 30 cm upstream from the window, had melted springs at the cycle end, indicating that its springs reached over 1350°C during service. This observation provides some idea of the magnitude of the temperature, but the exact temperature that the window itself reached during service is unknown. Overall, this

type of failure of the window from excessive thermal-mechanical stresses during service would certainly cause significant down time of the accelerator from the damage incurred.

1.3 Previous Isotope Production Facility Window Testing

Preliminary analysis was carried out on the 2010 IPF window in a hot cell. Samples were milled out of the window at regions of differing dosages. Shear punch testing was conducted on 21 samples. Dosages were determined using autoradiography and Monte Carlo N-Particle Transport Code eXtended (MCNPX) simulations. In the highest dose region (11.3 dpa), hardening was observed, as expected [5]. However, surprisingly, the lowest dosage samples (0.2-0.7 dpa), which were located on the outer edge of the window away from the beam spot, demonstrated the highest amount of hardening [5]. TEM analysis was conducted on the 11.3 dpa sample as well as the 0.7 dpa sample. γ" precipitates were found in the 0.7 dpa sample, which led to the high level of hardening. However, no precipitates were found in the 11.3 dpa region, which accounts for the 11.3 dpa region being weaker relative to the 0.7 dpa region. Several hypotheses were presented to explain why the lower dosage region formed precipitates, while the higher region did not, one of which was that the higher dose region formed precipitates at a low dose, which then disordered after further irradiation.

The aforementioned behavior initially motivated this study. Systematically investigating the evolution of the microstructure would allow us to determine the evolution of the precipitates. However, near the end of this study, it was determined that the 2010 beam window was initially precipitation hardened (PH), not annealed as previously

thought, which accounted for the discrepancies. As the window was irradiated, the precipitates would have become disordered. At lower doses, such as the 0.7 dpa sample that was tested, the precipitates did not fully disorder. However, at the high dose regions, the precipitates fully disordered. This accounts for the high hardening in the low dose region, and relatively low hardening in the high dose region.

Because the IPF designs typically call for annealed Alloy 718 in the designs, the results of this study will remain useful in future windows to understand the microstructural evolution.

1.4 Alloy 718 Properties and Microstructure

The composition ranges for Alloy 718 are outlined in Specification AMS 5596A, and are listed in Table 1 below. Additionally, Appendix A contains the composition analysis on the Alloy 718 that was used to fabricate the samples used in this study. Composition is well within the bounds established in Table 1.

Table 1. Allowable Atomic Weight Percent Ranges for Alloy 718 [2]

Composition		Element						
	Cr	Ni+Co	Mo	Nb+Ta	Ti	Al	B	Fe
Wt %	17.00-21.00	50.00-55.00	2.80-3.30	5.00-5.50	0.65-1.15	0.40-0.80	0.0020-0.0060	Balance
	C	Mn	Si	P	S	Co	Cu	
Wt %	0.03-0.10	0.35 max	0.35 max	0.015 max	0.015 max	1.00 max	0.10 max	

Alloy 718's microstructure consists of a matrix γ; precipitates γ", γ', and δ; and carbides. The matrix γ is FCC structured, consisting of a solid solution of the alloying elements. The γ" precipitates are disk shaped with composition $Ni_3(Nb,Ti)$, which is a metastable phase with a tetragonal space centered structure (DO_{22}). γ" precipitates are thought to account for the majority of Alloy 718's strengthening through coherency hardening [6]. At high temperatures, the γ" phase transforms into the stable orthorhombic δ phase, which is known to be incoherent with the matrix [7]. Small amounts of the γ' phase are also present; these particles are spherical and exhibit $L1_2$ structure with the composition $Ni_3(Al,Ti,Nb)$. However, because the volume fraction is so low, this phase has little effect on the alloy's properties [8].

1.5 Overview of the Effect of Irradiation on Metals

In 1946 Wigner was the first to predict that neutron bombardment would cause displacement of atoms from their regular lattice positions, which would in turn alter the material's properties; this prediction was later experimentally confirmed [9]. Radiation effects can be caused by three interactions: nuclear reactions, elastic collisions, and electronic excitations [10]. In metals, electronic excitations manifest as heat, leaving nuclear reactions and elastic collisions as the main interaction types. For Inconel in the energy range of this study, nuclear reactions are not applicable. Therefore, elastic scattering is the relevant mechanism of interest here. Elastic collisions involve the irradiating ion transferring energy to the first lattice atom with which it interacts, which is

known as the primary knock-on atom (PKA). If the PKA receives energy in excess of some threshold energy, the PKA will leave its lattice site and create a Frenkel defect [10]. With enough energy, the PKA can collide with other atoms, create new knock-on atoms, and thereby produce displacement cascades. This causes production of vacancies and interstitials, which is the principal cause of property changes, including swelling, hardening, and creep.

Hardening in metals, which is of particular interest in this study, is primarily due to dislocations acting as obstacles to movement [10]. Irradiated microstructures can be very complex and can include defect clusters, small dislocation loops, dislocation networks, voids, and precipitates, most of which act as obstacles to dislocation movement. Void swelling is typically observed at irradiation temperatures between 0.3-0.6T_m, or 210°C-692°C for Alloy 718 [10]. As will be discussed in the following sections, the irradiation temperatures for this experiment fall below this threshold. As such, void swelling is unlikely to play a key role here. Instead, we are left with the possibility of defect clusters, loops, dislocation networks, and precipitates as playing key roles.

Friction hardening is the stress required to maintain dislocation movement and is due to the presence of clusters, loops, dislocation networks, and precipitates. These hardening sources can be either short range or long range, and contribute to the total applied shear stress required to move a dislocation. In a single crystal, this total stress is given by [11]:

$$\sigma_F = \sigma_{LR} + \sigma_{SR} \tag{1}$$

where the subscript F represents the friction stress, LR represents long range, and SR represents short range. Long range stress derives from the repulsive behavior between a dislocation and the dislocation network. The long range stress can be written as [11]:

$$\sigma_{LR} = \alpha \mu b \sqrt{\rho_d} \tag{2}$$

where α is a constant typically less than 0.2, μ is the shear modulus, b is the magnitude of the Burgers vector, and ρ_d is the dislocation density (in number per square length).

Neglecting the effect of voids, as they are not expected to play a key role here as described above, the short range stress is given by Equation 3 [11].

$$\sigma_{SR} = \sigma_{precipitates} + \sigma_{loops} \tag{3}$$

$\sigma_{precipitates}$ and σ_{loops} in Equation 3 can each be expressed in the form of Equations 4 and 5:

$$\sigma_{precipitates} \approx \alpha_{precipitates} M \mu b \sqrt{Nd} \tag{4}$$

$$\sigma_{loops} \approx \alpha_{loops} M \mu b \sqrt{Nd} \tag{5}$$

where α is a dimensionless parameter related to dislocation strength, μ is the shear modulus, b is the magnitude of the Burgers vector, M is the Taylor factor and is approximately 3.06, d is the diameter the given obstacle (precipitate or loop), and N is the number of the given obstacles (precipitates or loops) present per volume. $\alpha_{precipitates}$ varies between 1 for bowing and 0.3-0.5 for cutting, and α_{loops} varies between 0.25-0.5 [11].

These relationships can be extended to polycrystals by utilizing a modified Hall-Petch equation given by Equation 6:

$$\sigma_y = \sigma_F + \mu b \left(\frac{\beta\varepsilon}{d_{grain}}\right)^{1/2} \quad (6)$$

where σ_F is the friction stress due to dislocations (in a single crystal), ε is strain, and d_{grain} is grain diameter, and β is a measure of work hardenability due to dislocation channeling [11]. Dislocation channeling refers to regions of very high plastic strain surrounded by regions with almost no plastic strain. During straining, dislocation loops are dragged or annihilated, leaving dislocation free zones, which are preferred for dislocation glide and plastic strain, thus creating high plastic strain regions [12].

Assuming that the material does not work harden, the hardness and yield strength are (approximately) directly related through Equation 7:

$$H \approx k\sigma_y \quad (7)$$

where the constraint factor k usually varies between 2.8-3.0 [11, 13].

1.6 Review of Studies on Irradiated Alloy 718

1.6.1 Irradiated Alloy 718 Mechanical Properties

Several studies have been completed on irradiated Alloy 718, but comparisons are difficult due to the unique conditions employed in each test. Ward et al. irradiated precipitation hardened (PH) Alloy 718 from 2-22 dpa with neutrons, while increasing the irradiation temperature from 404°C to 649°C with dosage. (Ward et al. reported fluences. Dosage equivalents were reported by LANL [14]). They found increased strength in both the samples irradiated to low fluences at low temperatures and in the samples irradiated to high fluences at high temperatures. Due to this behavior, it was concluded that competing

mechanisms of thermal overaging and irradiation hardening were occurring, meaning that the higher dosage reversed the hardening seen in lower dosages [15].

Maloy et al. analyzed the effect of high energy proton and neutron irradiation (800 MeV) on PH Alloy 718, to a maximum dose of 12 dpa. Irradiation temperatures varied from 50-164°C. It was found that the yield strength increases by 100-200 MPa with dose up to 1 dpa, and then gradually decreases up to 12 dpa [16]. Citing a study by Sencer et al., the reduction in yield strength after 1 dpa was attributed to irradiation-induced disordering of the hardening precipitates, γ" and γ' [17].

James et al. at LANL investigated the properties of a PH Alloy 718 beam window that had been irradiated at IPF for two years [14]. Specifically, the maximum dose in the window was found to be 20 dpa. Dog-bone tensile specimens were cut from the window at several different dosages. Although the preparation and testing methods varied, the general results agreed with that of Ward et al. and Maloy et al. The maximum observed strength was found at about 2 dpa, with decreasing yield strength thereafter. This study also carried out microhardness testing using a diamond pyramid under a 400 g load. Results agree with that seen in the tensile tests. Locations near the center of the window (high dose) exhibited decreased hardness compared to the edge of the window, which is approximately still in the PH state. For samples taken from the center of the window (highest dose), the hardness appeared to rise again (while still remaining softer than the PH state), which was attributed to embrittlement.

Byun and Farrell investigated the effect of neutron irradiation on both solution annealed Alloy 718 and PH Alloy 718 at 60-100°C [18]. It was hypothesized that the

annealed Alloy 718 would exhibit significant hardening due to radiation, and possibly would retain better ductility. Samples were irradiated to a range of dosages, from 0.00057 to 1.2 dpa. The annealed Alloy 718's yield strength increased strongly with dose; at 1.2 dpa, the yield strength was almost three times higher than the unirradiated state. However, the change in yield strength of the PH Alloy 718 was much more subdued. As predicted, the annealed Alloy 718 retained significant ductility (up to 20% at 1.2 dpa) [18].

Overall, studies such as these have reinforced that dissolution of γ" and γ' precipitates is a significant factor in the behavior of PH Alloy 718.

1.6.2 TEM Analysis of Irradiated Alloy 718 in the Annealed and PH Conditions

Hashimoto et al. characterized TEM microstructure for irradiated Alloy 718 beginning in the PH and annealed conditions [19]. Samples were irradiated with Fe ions at 200°C to dosages ranging from 0.1-10 dpa. For annealed Alloy 718, this study observed Frank-type faulted loops at the higher dosages. For the precipitation hardened Alloy 718, the γ" and γ' superlattice diffraction patterns had disappeared by 1.0 dpa, therefore confirming that softening is due to the dissolution of the γ" and γ' precipitates. Above 1 dpa, the PH Alloy 718 exhibited a high number of Frank-type faulted loops. However, it appears that the disordering of the precipitates played a more significant role, since the samples experienced a net softening.

While it is apparent that extensive previous work has been carried out to characterize irradiated Alloy 718 beginning in the PH condition, only two studies were carried out that investigated irradiated Alloy 718 that began in the annealed state [18, 19].

To this end, we performed further systematic investigation of Alloy 718 beginning in the annealed state.

CHAPTER II

RESEARCH OBJECTIVES AND SAMPLE PREPARATION

The purpose of this study is to characterize the evolution of the microstructure and mechanical properties of irradiated Alloy 718. This study is unique from most studies on irradiated Alloy 718 in the literature for several reasons, but most importantly because the Alloy 718 in this study is annealed, not precipitation hardened, prior to irradiation. This approach is heavily motivated by the fact that the Alloy 718 window at IPF enters the beamline in the annealed state. Therefore, through the range of irradiation temperatures, annealing temperatures, and dosages in this study, we aim to imitate and examine the microstructural evolution that the IPF window experiences during use, and further determine if in-situ annealing of the Alloy 718 window will extend its life. If feasible, in-situ annealing will cut down significantly on costs associated with physically replacing the window as well as those related to beam downtime during the replacement process.

In line with this goal, irradiation temperatures and annealing temperatures were chosen that are representative of those achievable at IPF. The matrix of irradiation and annealing temperatures is shown in Table 1. The 3 mm diameter samples began in the annealed condition.

Table 2. 15 DPA Irradiation Parameters

Room Temp Irradiation + No Anneal	100°C Irradiation + No Anneal	200°C Irradiation + No Anneal
Room Temp Irradiation + 300°C Anneal	100°C Irradiation + 300°C Anneal	200°C Irradiation + 300°C Anneal
Room Temp Irradiation + 500°C Anneal	100°C Irradiation + 500°C Anneal	200°C Irradiation + 500°C Anneal

Table 3. 0.5-0.67 DPA Irradiation Parameters

100°C Irradiation + No Anneal
100°C Irradiation + 300°C Anneal
100°C Irradiation + 500°C Anneal

This matrix of irradiation and annealing parameters will allow us to see how the parameters evolve with dosage as well as with the irradiation and annealing temperatures. All anneals were carried out in vacuum or in an argon gas environment for 1 hour. Due to the achievable depths of penetration as well as the length of time required for irradiation, 15 dpa was carried out with Ni ions. This irradiation was completed at 5 MeV. The average dosage between 0.8 and 1.8 μm was 15 dpa, and thus 0.8-1.8 μm is the region of interest for the 15 dpa samples. The dosage curve can be seen in Figure 4, with vertical bars indicating the region of interest. Data to construct this curve was calculated in SRIM

(Stopping Range of Ions in Matter) 2013 with 5.0 MeV Nickel ions implanting into Nickel. Similar simulations were also run including more of the alloying elements found in Alloy 718. This was found to have minimal effect, so the simpler model was chosen. The 15 dpa samples were irradiated 3 at a time, and adhered to the stage using silver paste. Calibration testing indicated that the samples were held within 5 degrees of the target temperature.

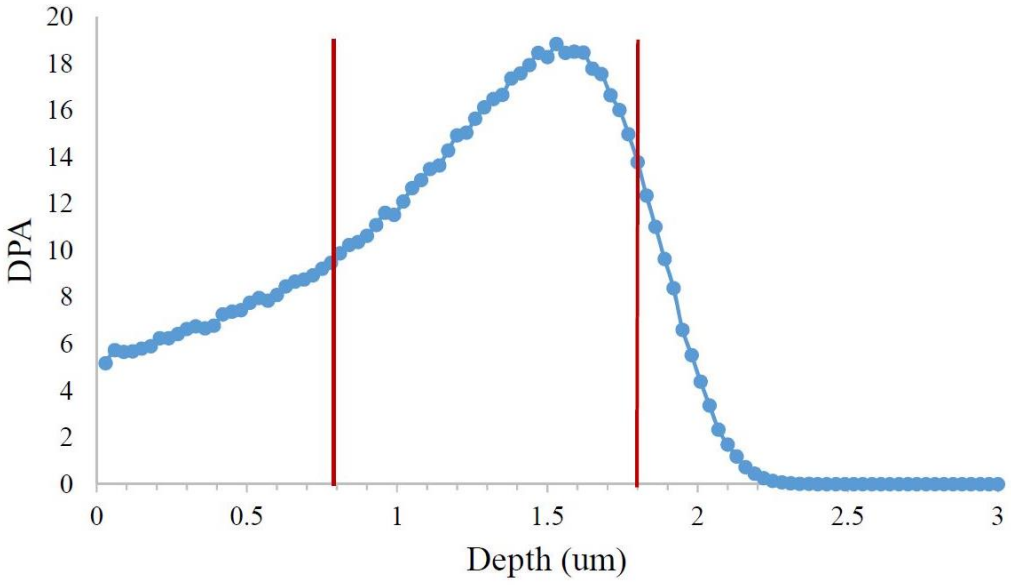

Figure 4. Dosage Curve and Region of Interest for 15 dpa Nickel Ion Irradiation

The 0.5 dpa samples were carried out with protons at 1.5 MeV. Because the irradiation time was considerable (approximately 22 hours), the matrix was reduced to three samples at a single irradiation temperature with three different annealing temperatures. Additionally, due to variations, the 100°C irradiation without annealing was 0.5 dpa, while the 100°C irradiation, 300°C and 500°C anneals were at 0.67 dpa. Figure 5 depicts the dosage curve for the 0.5 dpa samples. Similarly to the 15 dpa samples, SRIM

2013 was used calculate information for the dosage curve, using 1.5 MeV protons and Nickel as the target. Again, simulations were also ran that included more of the Alloy 718 alloying elements, but the addition of the alloying elements did not make significant difference in the dosage curve. The region between 1 and 6 μm has an average dose of 0.5 dpa, and thus the depth of interest for the 0.5 dpa samples is 1-6 μm. This region is indicated on Figure 5 with vertical lines. Due to difficulty maintaining 100°C sample temperature, the backs of the samples were lined with silver paste and then pressure fit using a TEM stage. This approach aided in ensuring the samples could be cooled to 100°C during irradiation. We currently do not have data on the variation in temperature during the irradiation but we know that the actual anneals were held at 274°C and 477°C, instead of 300°C and 500°C, respectively.

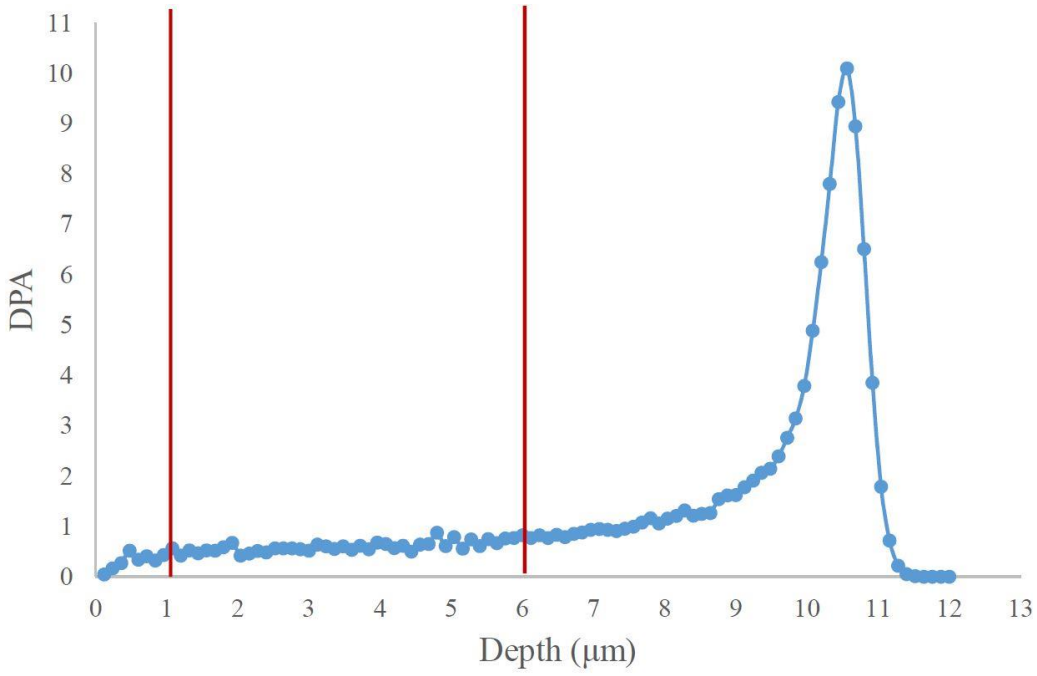

Figure 5. Dosage Curve and Region of Interest for 0.5 dpa Proton Irradiation

In addition to these 12 samples, 3 samples were used as controls. These were an unirradiated sample, an unirradiated 300°C annealed sample, and an unirradiated 500°C annealed sample. Thus, the total matrix included 15 samples.

The objective was to characterize several properties of these samples, namely nanoindentation to measure hardness (and elastic modulus) of all of the samples. TEM was used determine the presence of precipitates and the relative dislocation densities between a subset of the samples.

CHAPTER III

NANOINDENTATION RESULTS

Nanoindentation was performed on all 15 samples included in this study, using a Nanomechanics, Inc. iMicro nanoindenter with a Berkovich tip and the continuous stiffness measurement (CSM) technique [20]. Relevant parameters for both the 0.5 and 15 dpa samples can be found in Appendix B. Each sample was mounted to an aluminum puck using Crystalbond for testing. After hardness testing, the unirradiated sample was optically imaged to quantify pileup around the indent. If significant sink in or pileup is present, it must be accounted for in order to produce accurate hardness results. The presence of pileup was examined by measuring the final cross sectional area of the indent (Figure 6) and comparing it to the final area calculated by the iMicro, based on the known geometry of the indenter tip. The average percent difference between the imaged area and area used for calculations was found to be about 3.75%. Therefore, pileup is not a significant factor in nanohardness measurements for this material, and correction was not required.

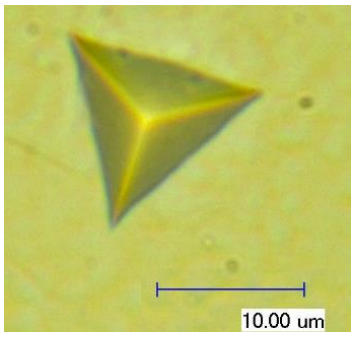

Figure 6. Example of Optically Imaged Indent

3.1 Nanoindentation Results – 15 dpa

The nine 15 dpa samples and the unirradiated sample were indented to two microns in depth. Seven tests were conducted on each sample, and the seven tests were averaged into one representative curve per sample. Figures 7, 8, and 9 show the representative load vs depth curves for the room temperature, 100°C, and 200°C irradiations. These curves appear as quite standard load-depth curves without any peculiar features, providing evidence as to the validity of the tests. The close groupings of curves indicate that none of the tests involved incorrect surface finds or similar (e.g., indenting into some foreign particle on the sample's surface) that would drastically and incorrectly alter results.

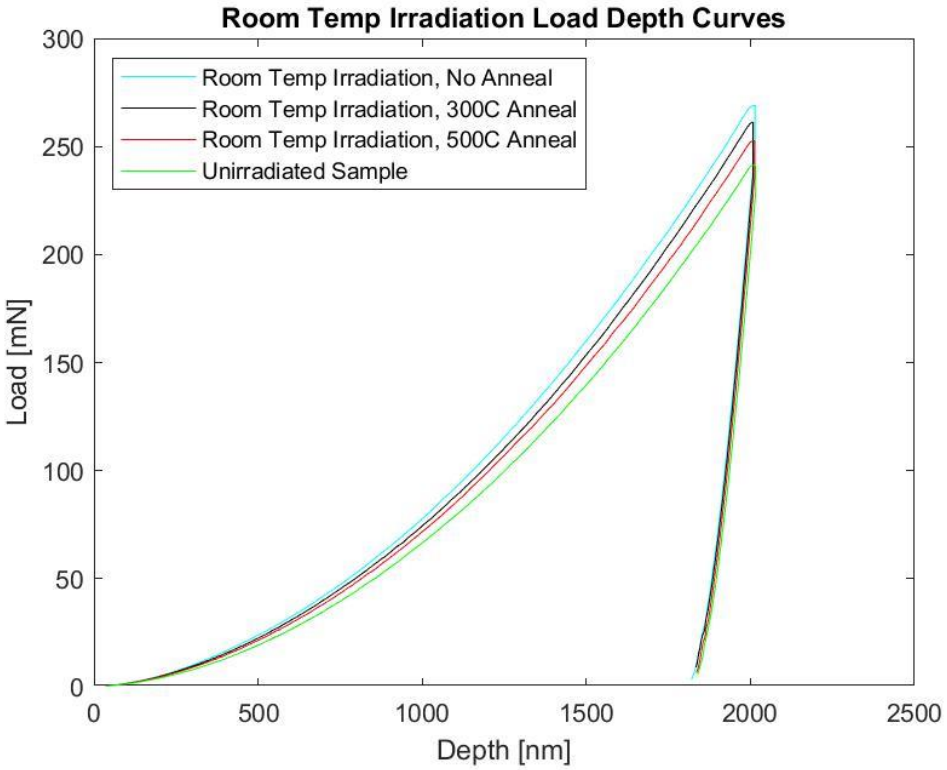

Figure 7. Room Temperature Irradiation Load Depth Curves (15 dpa)

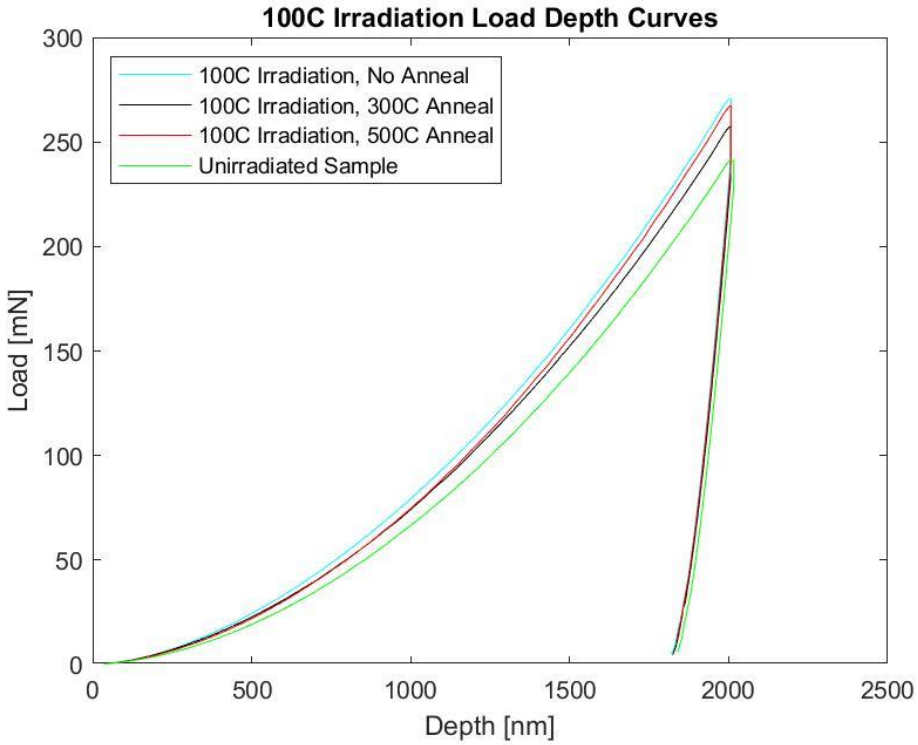

Figure 8. 100°C Irradiation Load Depth Curves (15 dpa)

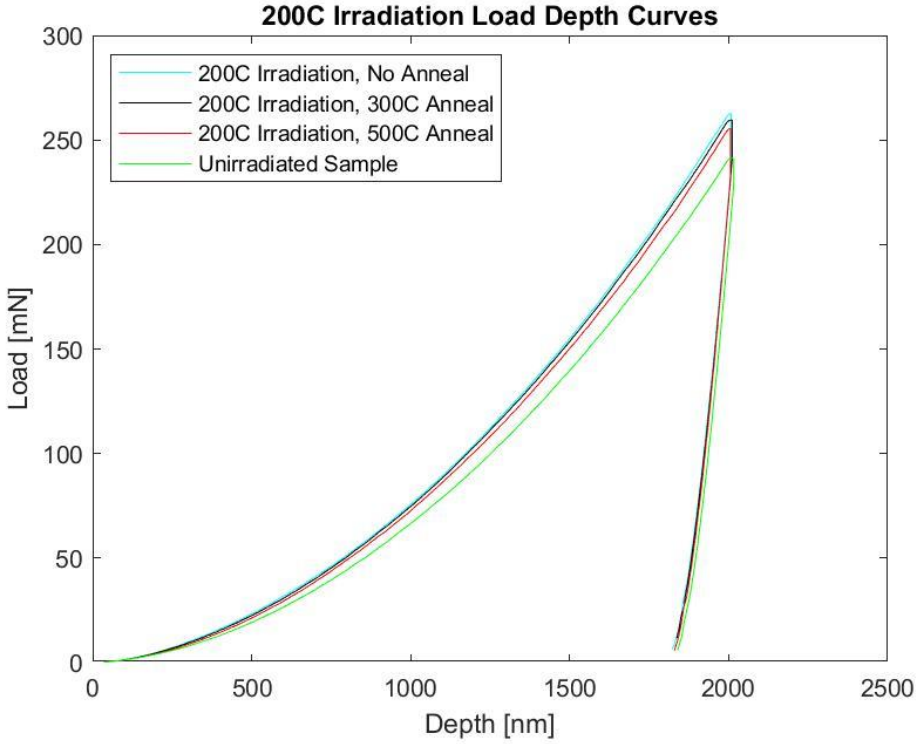

Figure 9. 200°C Irradiation Load Depth Curves (15 dpa)

From these load-depth curves, curves representing the elastic modulus versus depth were produced using the Oliver-Pharr method [21]. These are shown in Figures 10-12, with mean values along with error bars representing one standard deviation from the mean. These graphs show that the elastic modulus does not depend on depth or irradiation temperature. This result was expected, as the elastic modulus depends almost solely on atomic bond strength. Although nickel ions were implanted into the material, slightly changing the composition, it was not expected to significantly alter the bond strengths because the material remains fairly homogeneous. Therefore, it is reasonable that the modulus is constant. Additionally, the average elastic modulus for Alloy 718 is 204 GPa [22]. This is less than 8% difference from the modulus found in the 15 dpa tests. As the irradiating species was not expected to change the modulus significantly, these results appear reasonable.

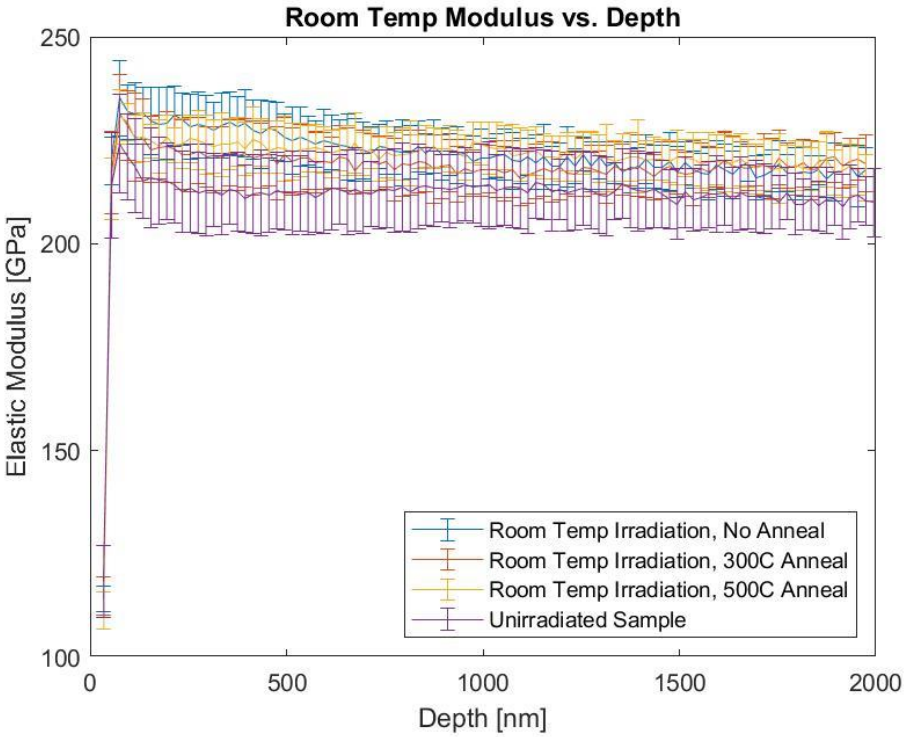

Figure 10. Modulus of Elasticity vs. Depth for Room Temperature Irradiations (15 dpa)

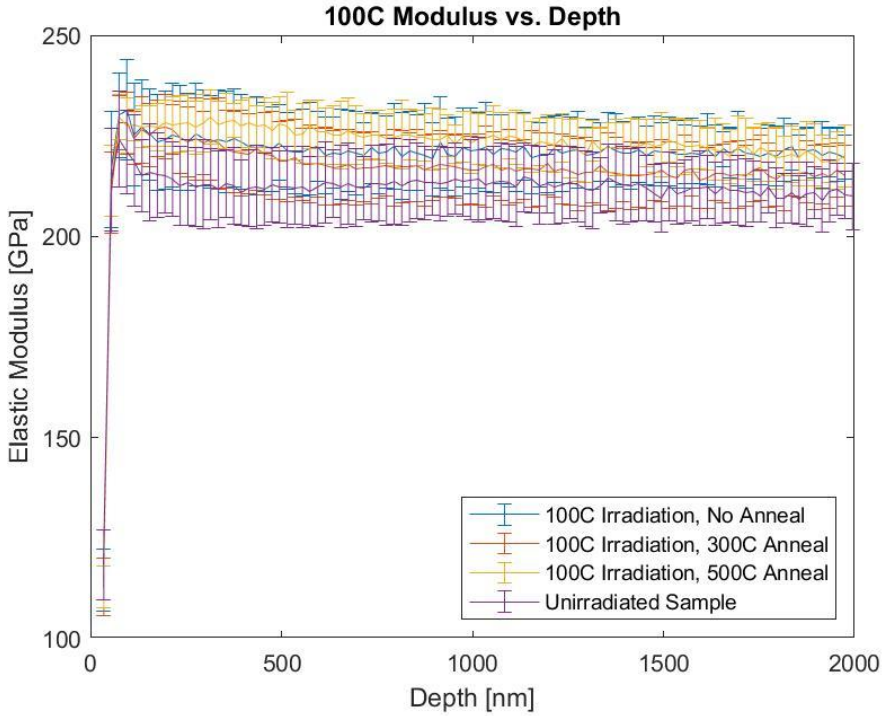

Figure 11. Modulus of Elasticity vs. Depth Curves for 100°C Irradiations (15 dpa)

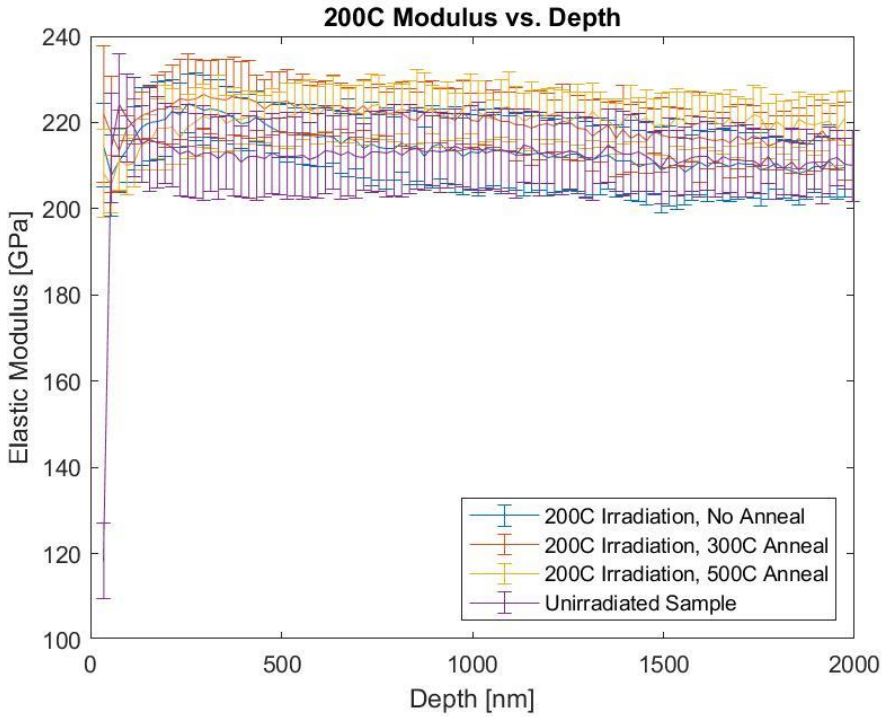

Figure 12. Modulus of Elasticity vs. Depth Curves for 200°C Irradiations (15 dpa)

Hardness data was also collected from nanoindentation testing. It is important to note that hardness can be seen to converge near the end of the region of interest. Nanoindentation probes not only the current depth, but also the entire plastic region, which extends up to five to ten times the penetration depth for metals [23, 24]. For example, this means that for a 200 nm indent, the reported hardness is actually influenced by the next one to two microns below that indent. For irradiated samples, this is significant, since the dose changes with depth. If we assume that the plastic zone here is five times the contact depth, a 500 nm indent includes data from the next 2.5 microns into the sample; that is, a 500 nm measurement is representative of the ~0.5-3.0 μm region in the sample. This encompasses our irradiated region of interest (and more). While this means that our hardness values are influenced by the unirradiated region, which begins at roughly 2.1

microns, hardness values below about 200 nm exhibit artificially high hardness due to indentation size effect, which may be caused by deformations induced by polishing and excessive sample roughness [25, 26]. Because of this, the trends in hardness will be taken at 500 nm, to avoid the artificially high hardness, while still sampling a region that is highly influenced by the dosage of interest. However, to determine the true hardness values associated with 15 dpa, indenting the cross section of the sample would be necessary, such that the dose does not change with depth. Unfortunately, doing so was not practical on this sample set, as the depth of interest is too shallow. In particular, an indentation produced by a nanoindenter has a width that is multiple times that of the depth. As such, trying to cross-section the sample and indent at exactly 1-2 μm from the surface would not be possible because the width of the indent would be larger than 2 microns (and thus even go 'off' of the sample), e.g., see Figure 6.

Hardness curves are shown in Figures 13-16. For all three irradiation temperatures, the hardness decreases with increasing irradiation temperature at 500 nm. Additionally, at 2000 nm, the hardness of the irradiated samples converges with that of the unirradiated sample. This lends credibility to this data, since upon indenting past the irradiated region, we expect to see properties of the unirradiated material.

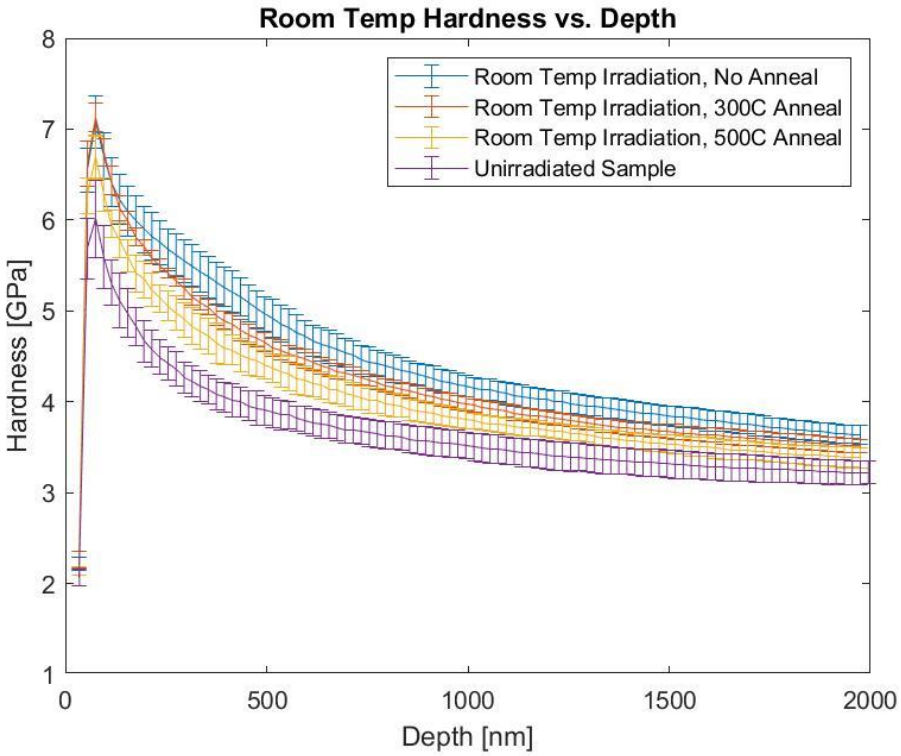

Figure 13. Hardness vs. Depth Curves for Room Temperature Irradiations (15 dpa)

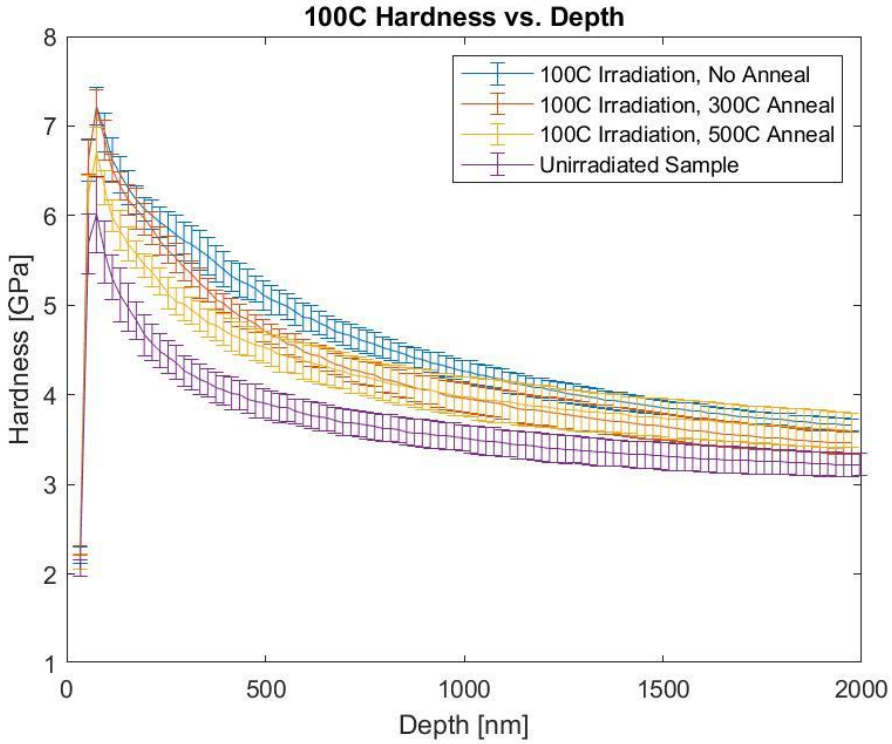

Figure 14. Hardness vs. Depth Curves for 100°C Irradations (15 dpa)

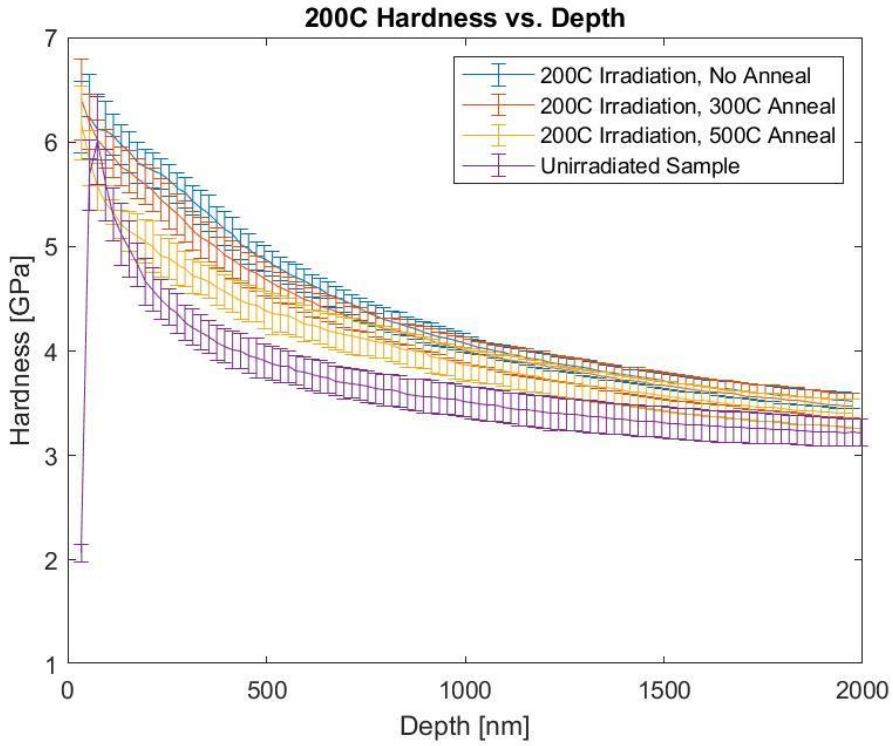

Figure 15. Hardness vs. Depth Curves for 200°C Irradations (15 dpa)

Finally, for a given annealing temperature, the hardness curves were plotted. As can be seen in Figure 16, the hardness curves at all irradiation temperatures are nearly identical. This also holds true for the no annealing and 500°C annealing cases, which are included in Appendix C. This indicates that the main change in properties is due to the change in annealing temperatures, which were larger than the temperatures from irradiation. Thus, the change in irradiation temperature had minimal effect on the properties.

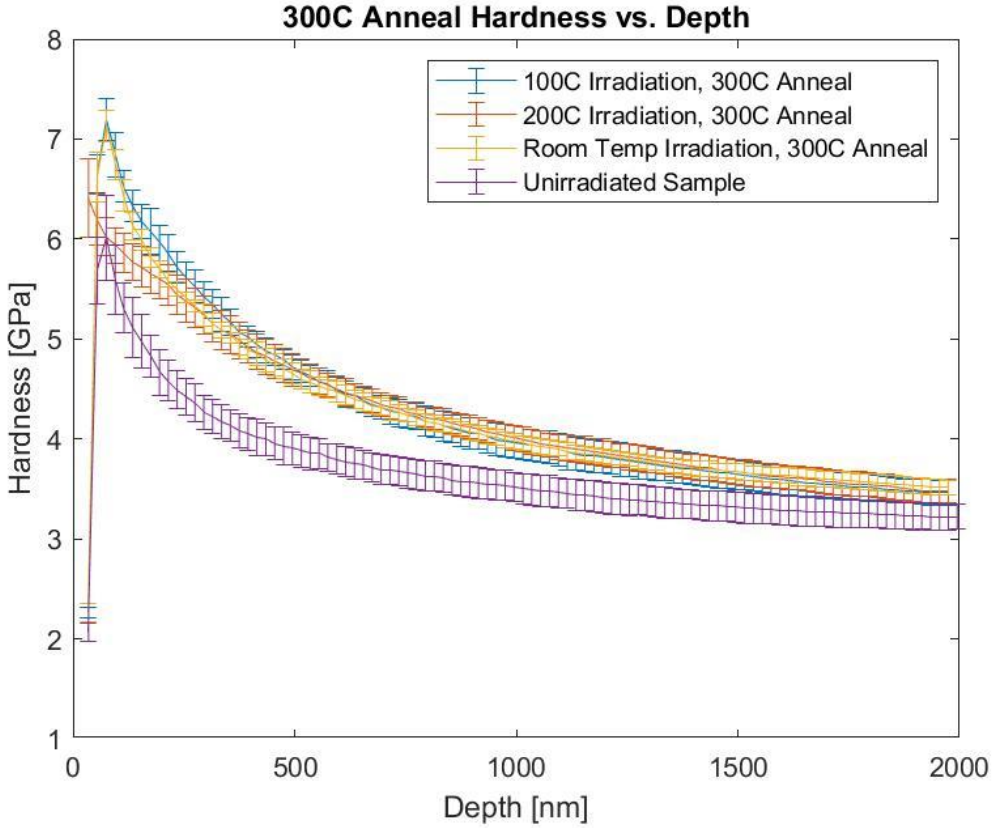

Figure 16. Hardness vs. Depth Graphs at Varying Irradiation Temperature (15 dpa)

3.2 Nanoindentation Results – 0.5 dpa

Using the same approach and conditions as for the 15 dpa samples, nanoindentation was performed on the 0.5 dpa irradiated samples. In this case, the irradiated region of interest existed between 1 and 6 μm. However, the iMicro nanoindenter used for this research had a maximum load of 1.0 N, which practically translated to a maximum depth of about 3 μm. With this constraint, for consistency of comparison with the 15 dpa samples, the tests were again performed to a maximum depth of 2 μm.

Similar to the 15 dpa samples, the modulus is essentially flat with depth, and the values overlap within the standard deviation of the tests for all of the annealing temperatures. This, again, is reasonable because the material is fairly homogenous, even when irradiated, and the bond strength is not expected to change due to irradiation. Additionally, the modulus is still in a reasonable range, as the reported value is about 204 GPa [22].

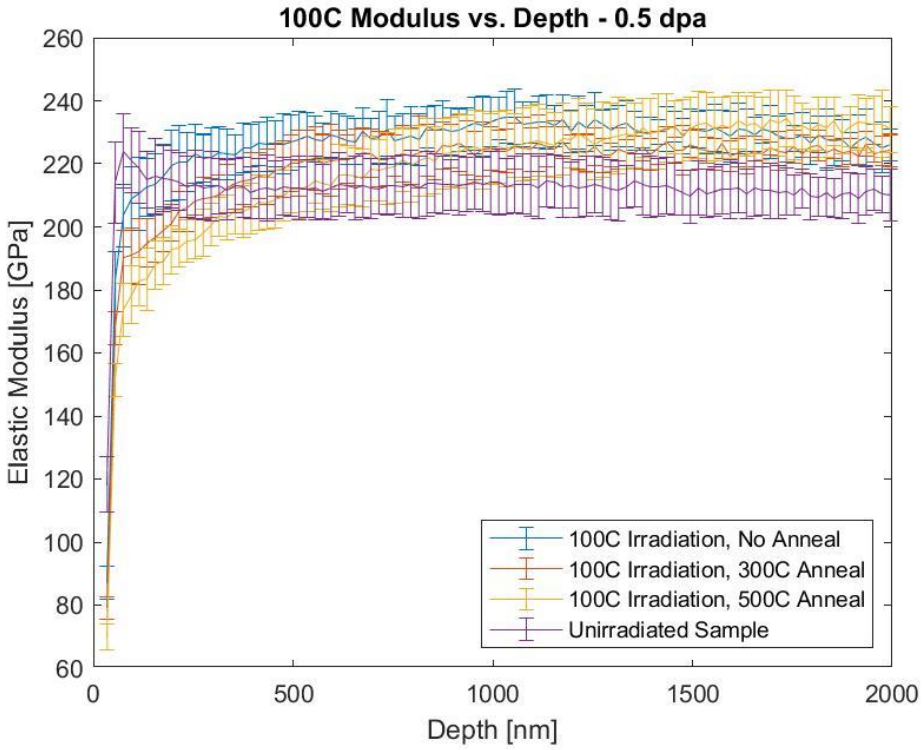

Figure 17. Elastic Modulus vs. Depth for 100°C Irradiations (0.5 dpa)

As discussed previously with the 15 dpa samples, depths below 200 nm exhibit artificially high hardness due to indentation size effect. Additionally, if we again assume that the plastic zone is up to five times the contact depth, an indent 1 micron in depth is

representative of 1-6 microns into the surface. Based on the dose profile seen previously in Figure 5, the 1-6 micron region has an average dose of 0.5 dpa; thus, observing hardness trends at 1 micron will produce meaningful information relevant to this dosage range.

Figure 18 shows the hardness vs. depth curves for the 100°C irradiations. At 2 μm, it is evident that the hardness values of the irradiated and unirradiated samples do not converge. This is to be expected, because the iMicro was unable to indent far enough into the sample such that the unirradiated area significantly influenced the measurements. Still, the trends in these tests seem to follow the trends from the 15 dpa samples: increasing annealing temperature results in decreased hardness, trending towards the unirradiated sample. However, there is overlap between the no anneal and 300°C anneal samples, and a clear difference exists between those and the 500°C anneal sample, which is unique to this dosage. One explanation for this could be that the dislocations were significantly more heavily affected by annealing at 500°C than 300°C. This theory could be confirmed by TEM analysis on all of the 0.5 dpa samples.

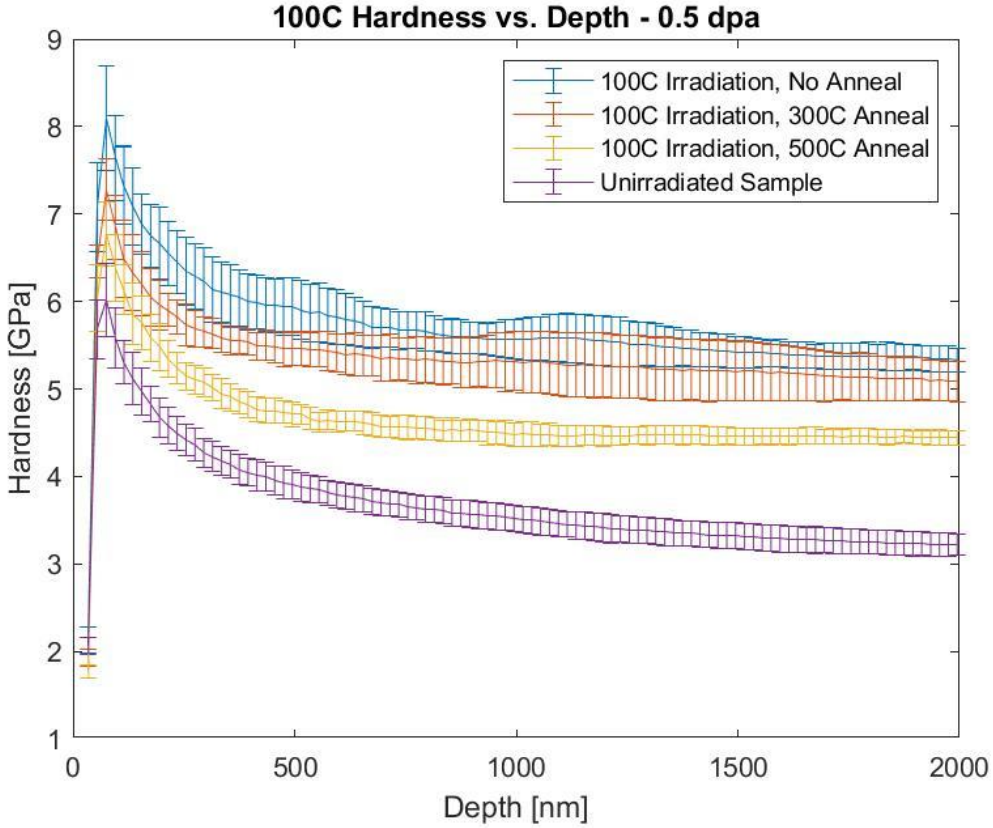

Figure 18. Hardness vs. Depth Curves for 100°C Irradiations (0.5 dpa)

CHAPTER IV

TEM ANALYSIS

The motivation for TEM analysis at the onset of this study was to determine why lower dose samples were harder than higher dose samples in the 2010 IPF window. It was hypothesized that this was due to the presence of precipitates. Once it was determined that this behavior was due to the use of PH Alloy 718, the motivation changed. Based on the hardness results in this study, we wanted to determine the cause of the trend of decreasing hardness with increasing annealing temperature. For completeness, both the presence of precipitates and the relative dislocation densities were analyzed.

TEM lamellas were prepared via Focused Ion Beam (FIB), by first depositing a layer of platinum on the Alloy 718 surface and trenching out on both sides of the platinum. This process was followed by thinning the remaining wall of 718, lifting it out, and mounting it on a TEM grid, as can be seen in Figure 19.

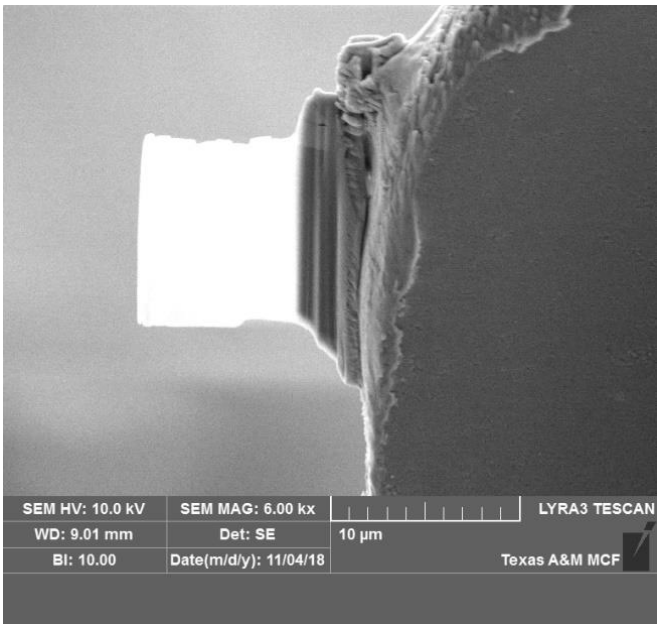

Figure 19. Example TEM Lamella

TEM lamellas were prepared on the ‘extreme conditions’ of the 15 dpa samples, which included the following:

- Room temperature irradiation without annealing (15 dpa)
- Room temperature irradiation with 500°C annealing (15 dpa)
- 100°C irradiation without annealing (15 dpa)
- 100°C irradiation with 500°C annealing (15 dpa)
- Unirradiated sample

The 200°C irradiation samples were excluded from this analysis as the IPF facility would unlikely be able to maintain that irradiation temperature in practice, and thus the room temperature and 100°C irradiated samples were of more direct practical relevance.

TEM analysis was conducted on all of the above samples in search of precipitates. No precipitates were found in any of the samples except the room temperature irradiation

with 500°C anneal sample, in which we observed a single precipitate present on a grain boundary about 950 microns into the depth, as shown in Figure 20. It is approximately 130 nm by 90 nm. Energy dispersive X-ray spectroscopy (EDS) in scanning transmission electron microscopy (STEM) mode enabled chemical mapping of the precipitate and the surrounding area, as shown in Figure 21. The presence of high concentrations of niobium and titanium and low concentrations of nickel compared to the matrix do not match the composition of γ" or γ'. As such, this precipitate does not seem to represent a typical hardening precipitate. Further diffraction information would be needed to fully characterize this precipitate, but further investigation of this precipitate was not carried out as precipitates were not prevalent in any of the samples. As such, their formation does not seem to play a significant role in the overall properties of our samples.

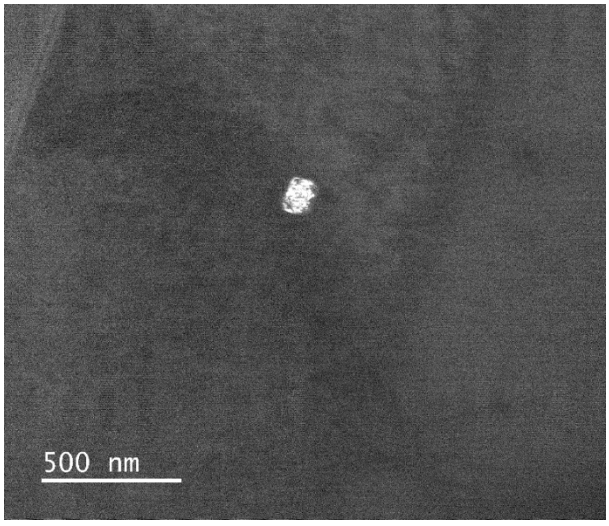

Figure 20. Precipitate in Room Temperature Irradiation, 500°C Anneal Sample (15 dpa)

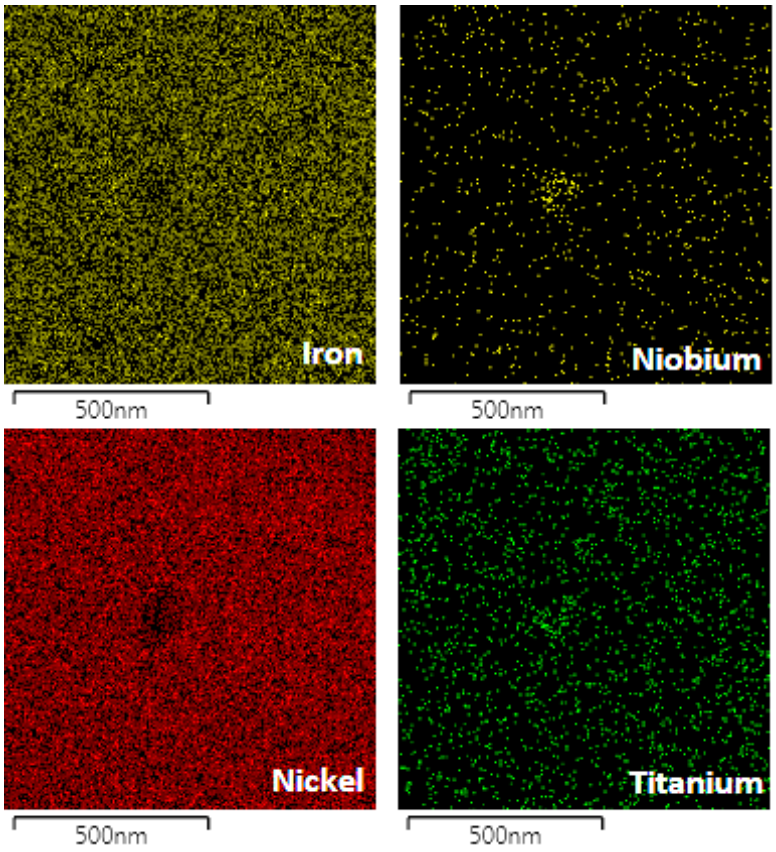

Figure 21. Chemical Composition of Precipitate and Surrounding Matrix

Because very few/no precipitates were present in the irradiated samples, the next step was to determine the mechanism causing the decrease in hardness. As such, the TEM (FEI Tecnai G2 F20 ST) was put in the two-beam condition, wherein only one diffracted beam is strong. Figures 22 and 23 both depict images of the room temperature irradiation with no annealing and 500°C annealing, respectively. Both images were captured at 20kx, and examples of dislocations are circled in red.

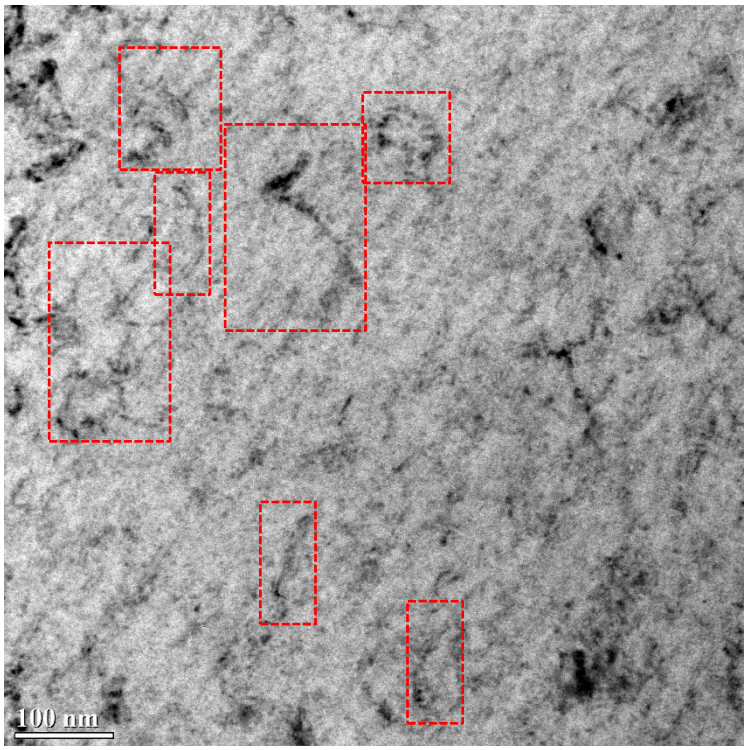

Figure 22. TEM Image of Room Temperature, No Anneal Sample (15 dpa)

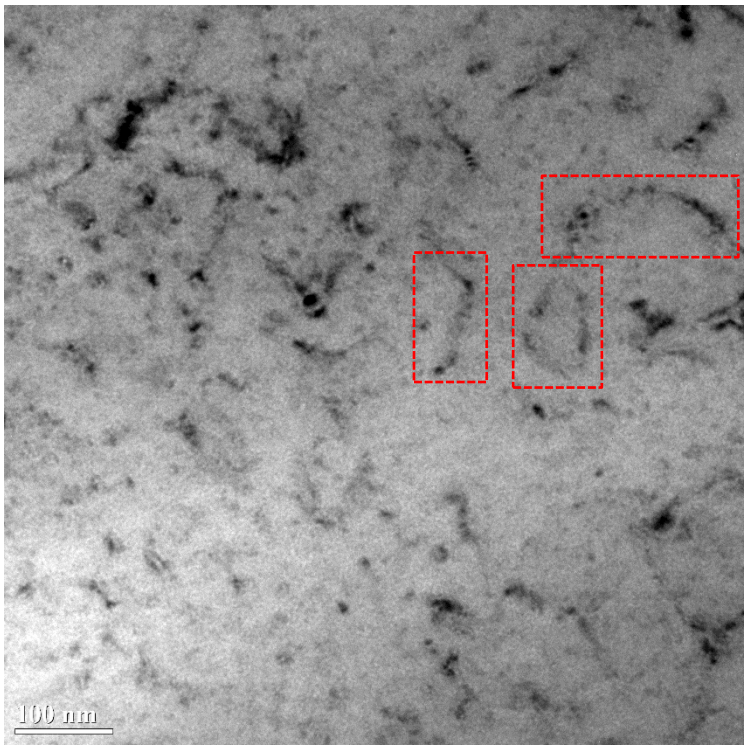

Figure 23. TEM Image of Room Temperature, 500C Anneal Sample (15 dpa)

At least qualitatively, it can be seen from Figures 22 and 23 that the annealed sample has a slightly lower dislocation density than does the unannealed sample. However, because the dislocation densities are on the same order of magnitude, it is not possible to conclusively state that dislocations are the cause of the decrease in hardness with increasing annealing temperature. However, it is possible to consider the quantitative effects of the microstructure on the hardness. Again, we have the long range stresses given by Equation 8, which is equivalent to Equation 2, with the assumption that α=0.15. From the aforementioned results, we found that precipitates are essentially not present in the material. Thus, they can be neglected in the analysis of short range stresses. Adapting Equations 3 and 5 with the assumption of α=0.3 and M=3.06 yields Equation 9, the short range stresses for this experiment.

$$\sigma_{LR} \approx 0.15\mu b\sqrt{\rho_d} \tag{8}$$

$$\sigma_{SR} \approx 0.198\mu b\sqrt{Nd} \tag{9}$$

Combining Equations 1 and 6-9 and assuming a constraint factor of 2.8 yields Equation 10, an equation for hardness in a polycrystal as a function of long and short range stresses due to dislocations.

$$H \approx 2.8\mu b\left(0.15\sqrt{\rho_d} + 0.198\sqrt{Nd_{loop}} + \sqrt{\frac{\beta\varepsilon}{d_{grain}}}\right) \tag{10}$$

If it is assumed that grain growth is minimal within the annealing temperatures (which were all less than half of the melting point) and with the one hour annealing times used, Equation 10 suggests that the difference in hardness as a function of annealing temperature is solely due to changes in dislocation density, number of loops per volume, and the size

of those loops. If we solely consider the effect of dislocation density on hardness, a factor of two increase in the dislocation density would produce a $\sqrt{2}$ or ~40% increase in hardness. Again, if we solely consider the effect of number of loops per volume or the diameter of these loops, a factor of two increase in either of these parameters would also cause a 40 percent increase in the hardness. Thus, it is readily apparent that for even small changes in dislocation density (i.e., not orders of magnitude changes), the number of loops per volume, and the diameter of the loops can have a marked impact on the resulting hardness.

If we return to the analysis of Figures 22 and 23, while the dislocation density has not changed by orders of magnitude, based on the above analysis, even this small change could reasonably account for the roughly 15 percent change in hardness between the room temperature irradiation no anneal and 500°C anneal samples at 500 nm in depth. To conclusively determine whether or not the decrease in dislocation density is the cause of the change in mechanical behavior, additional samples should be tested to determine if they support this trend. Specifically, the dislocation density of the 100°C and 200°C should be investigated, including thorough numerical quantification of dislocation density, number of dislocations per volume, and the average diameter of the dislocation loops.

CHAPTER V

FUTURE WORK

The preceding work could be extended in several ways in order to more thoroughly understand the microstructural evolution of irradiated Alloy 718 beginning in the annealed condition. First, more testing can be carried out on the samples already on hand. TEM lamellas can be prepared and analyzed for the 0.5 dpa samples; this would be useful in determining the mechanism that caused the 500°C annealed sample to have a significantly decreased hardness from the no anneal and 300°C samples. Additionally, it would be beneficial to conduct micropillar compression testing on the 0.5 dpa samples in order to construct a stress-strain curve for the materials. Such curves would provide useful information related to the behavior of these materials after yielding, such as the strain-hardening exponents. Additionally, indenting the 0.5 dpa samples through the cross section, would produce more reliable hardness data that is not influenced by other dosages. Finally, systematically determining the dislocation density quantitatively will provide the evidence needed to prove whether decreasing dislocation density caused the decrease in hardness.

Once all testing is complete on these samples, it may prove beneficial to investigate annealing at higher temperatures and/or for longer periods of time, to determine if the properties fully approach that of the unirradiated material. Such studies would provide direct utility to IPF if these further annealing studies are carried out to the temperatures and/or annealing times that they are capable of achieving at the facility. Likewise, it may

also be useful to expand the 0.5 dpa matrix to match that of the 15 dpa samples, that is, produce 9 total samples irradiated to 0.5 dpa.

As previously mentioned, conducting ABAQUS simulations of the indentation process using representative numbers for the modulus and hardness of annealed Alloy 718 would allow us to estimate the typical length scales of the elastic and plastic zones for this material. This would allow us to determine a reliable depth for hardness measurements that is truly representative of the irradiated region.

Finally, it may be beneficial to develop a new set of experiments to analyze the creep that potentially occurred in the 2010 IPF window. This window bulged into the vacuum side, which may be indicative of creep. Understanding the mechanisms and timescale by which this deformation occurred may be beneficial for IPF to investigate if this material is used in the future.

Implementing some or all of these tests would provide a more comprehensive understanding of the evolution of Alloy 718, beginning in the annealed condition. Such studies would allow a more definitive answer on whether or not annealing the Alloy 718 window at IPF is a feasible cost saving measure.

CHAPTER VI

CONCLUSION

This study aimed to systematically characterize the mechanical and microstructural evolution of irradiated Alloy 718 beginning in the annealed condition. The experiments involved a test matrix that includes 2 doses, 3 irradiation temperatures, and 3 annealing temperatures, for a total of 12 irradiated samples. The motivation for this study was twofold. First, LANSCE would like to determine if in-situ annealing is a feasible method to reverse the effects of radiation damage, and therefore decrease the frequency at which its beam window needs to be replaced. Second the study is aimed at providing a more comprehensive understanding of the microstructural changes developed in the Alloy 718 during radiation cycles.

Nanoindentation testing was carried out on all 12 irradiated samples and the controls. We determined that for a given irradiation temperature, the hardness decreased with increasing annealing temperature. The results also demonstrated that the irradiation temperature bore little to no effect on the hardness. TEM analysis performed on a subset of the higher dpa samples provided evidence of only one single precipitate among all samples (in the most extreme conditions), and it was thus determined that precipitation was not a key factor here. Following this study, additional TEM analysis was carried out to determine the mechanism by which annealing was decreasing hardness. Analysis of the room temperature irradiated 15 dpa samples (no anneal and 500°C anneal) showed that the annealed sample had a lower dislocation density. However, as the magnitude of this

density was the same between both samples, we were unable to conclusively determine that this was the cause of the change in mechanical properties.

Overall, this study indicates that in-situ annealing radiation damage out of the accelerator window at IPF is indeed feasible and promising. Future studies should focus on determining the exact annealing temperatures and times that are most effective in annealing this damage as to maintain long lifetimes.

REFERENCES

1. Mills, W.J., *Fracture Toughness Variations for Alloy 718 Base Metal and Welds.* The Metallurgical Society, 1989(Superalloy 718 Metallurgy and Applications (1989)): p. 517-532.
2. Wagner, H.J., A.M. Hall, and C. Defense Metals Information, *Physical metallurgy of alloy 718*. 1965, Columbus, Ohio: Defense Metals Information Center, Battelle Memorial Institute.
3. Sundararaman, M., S. Banerjee, and H. Mori, *The Stability of γ" and γ' Phases in Alloy 718 Under Electron Irradiation.* The Minerals, Metals, and Materials Society, 2001(Superalloys 718, 625, 706 and Various Derivatives (2001)): p. 379-387.
4. Saleh, T., et al., *Mechanical Properties of an Irradiated Inconel 718 Beam Window*. Los Alamos National Laboratory.
5. Bach, H.T., et al., *Proton irradiation damage of an annealed Alloy 718 beam window.* Journal of Nuclear Materials, 2015. **459**: p. 103-113.
6. Oblak, J.M., D.F. Paulonis, and D.S. Duvall, *Coherency strengthening in Ni base alloys hardened by DO22 γ' precipitates.* Metallurgical Transactions, 1974. **5**(1): p. 143-153.
7. Radavich, J.F., *The Physical Metallurgy of Cast and Wrought Alloy 718*. 2004. 229-240.

8. Jambor, M., et al., *Phase transformations in nickel base superalloy INCONEL 718 during cyclic loading at high temperature*. Vol. 15. 2017. 15-18.

9. Wigner, E.P., *Theoretical Physics in the Metallurgical Laboratory of Chicago.* Journal of Applied Physics, 1946. **17**(11): p. 857-863.

10. Ullmaier, H., *Radiation Damage in Metallic Materials.* MRS Bulletin, 1997. **22**(4): p. 14-21.

11. Was, G.S., *Fundamentals of Radiation Materials Science*. Vol. 2. 2007: Springer.

12. Onimus, F., et al., *A statistical TEM investigation of dislocation channeling mechanism in neutron irradiated zirconium alloys.* Journal of Nuclear Materials, 2004. **328**(2): p. 165-179.

13. Zhang, P., S.X. Li, and Z.F. Zhang, *General relationship between strength and hardness.* Materials Science and Engineering: A, 2011. **529**: p. 62-73.

14. James, M.R., et al., *The mechanical properties of an Alloy 718 window after irradiation in a spallation environment.* Journal of Nuclear Materials, 2001. **296**(1): p. 139-144.

15. Ward, A.L., J.M. Steichen, and R.L. Knecht, *Irradiation and Thermal Effects on the Tensile Properties of Inconel 718*, in *Irradiation Effects on the Microstructure and Properties of Metals*. 1976, American Society For Testing And Materials. p. 156-170.

16. Maloy, S.A., et al. *The Effect of High Energy Protons and Neutrons on the Tensile Properties of Materials Selected for theh Target and Blanket*

Components in the Accelerator Production of Tritium Project. in *Effects of Radiation on Materials: 20th International Symposium*. 2000. ASTM.

17. Sencer, B.H., et al. *Microstructural Alteration of Structural Alloys by Low Temperature Irradiation with High Energy Protons and Spallation Neutrons*. in *Effects of Radiation on Materials: 20th International Symposium*. 2000. ASTM.
18. Byun, T.S. and K. Farrell, *Tensile propeties of Inconel 718 after low temperature neutron irradiation.* Journal of Nuclear Materials, 2003. **318**: p. 292-299.
19. Hashimoto, N., et al., *Microstructural analysis of ion-irradiation-induced hardening in inconel 718.* Journal of Nuclear Materials, 2003. **318**: p. 300-306.
20. Li, X. and B. Bhushan, *A review of nanoindentation continuous stiffness measurement technique and its applications.* Materials Characterization, 2002. **48**(1): p. 11-36.
21. Oliver, W.C. and G.M. Pharr, *An improved technique for determining hardness and elastic modulus using load and displacement sensing indentation experiments.* Journal of Materials Research, 1992. **7**(6): p. 1564-1583.
22. *VDM Alloy 718 Data Sheet*. 2019.
23. Dolph, C.K., et al., *Plastic zone size for nanoindentation of irradiated Fe–9%Cr ODS.* Journal of Nuclear Materials, 2016. **481**: p. 33-45.
24. Hosemann, P., et al., *Issues to consider using nano indentation on shallow ion beam irradiated materials.* Journal of Nuclear Materials, 2012. **425**(1): p. 136-139.

25. Nix, W.D. and H. Gao, *Indentation size effects in crystalline materials: A law for strain gradient plasticity.* Journal of the Mechanics and Physics of Solids, 1998. **46**(3): p. 411-425.

26. Swadener, J.G., E.P. George, and G.M. Pharr, *The correlation of the indentation size effect measured with indenters of various shapes.* Journal of the Mechanics and Physics of Solids, 2002. **50**(4): p. 681-694.

APPENDIX A

COMPOSITION ANALYSIS

Combustion infrared detection was conducted for carbon and sulfur in accordance with ASTM E 1019-18. For all remaining elements, direct current plasma emission spectroscopy in accordance with ASTM E 1097-12 was used.

Sample Identification	Weight Percent
Carbon	0.057
Sulfur	0.0005
Nickel	53.21
Chromium	17.59
Iron	18.69
Niobium	5.03
Molybdenum	3.00
Titanium	1.02
Aluminum	0.58
Cobalt	0.17
Manganese	0.28
Silicon	0.088
Phosphorus	0.007
Boron	0.0042
Copper	0.27

APPENDIX B

NANOINDENTATION PARAMETERS

The parameters associated with the nanoindentation of the 0.5 and 15 dpa samples are as follows:

Target indentation strain rate:	0.050 [1/s]
Target frequency:	110 [Hz]
Target dynamic displacement:	2.00 [nm]

APPENDIX C

ADDITIONAL HARDNESS VS. DEPTH CURVES

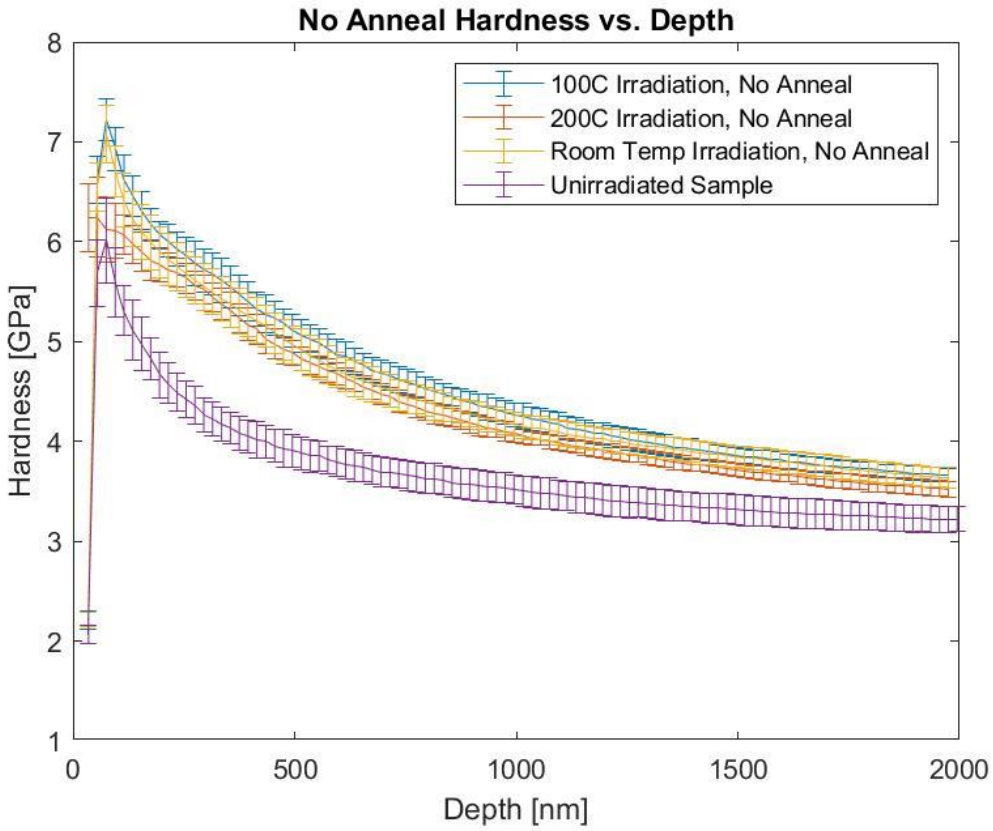

Hardness vs. Depth Curves for No Annealing for Several Irradiation Temperatures

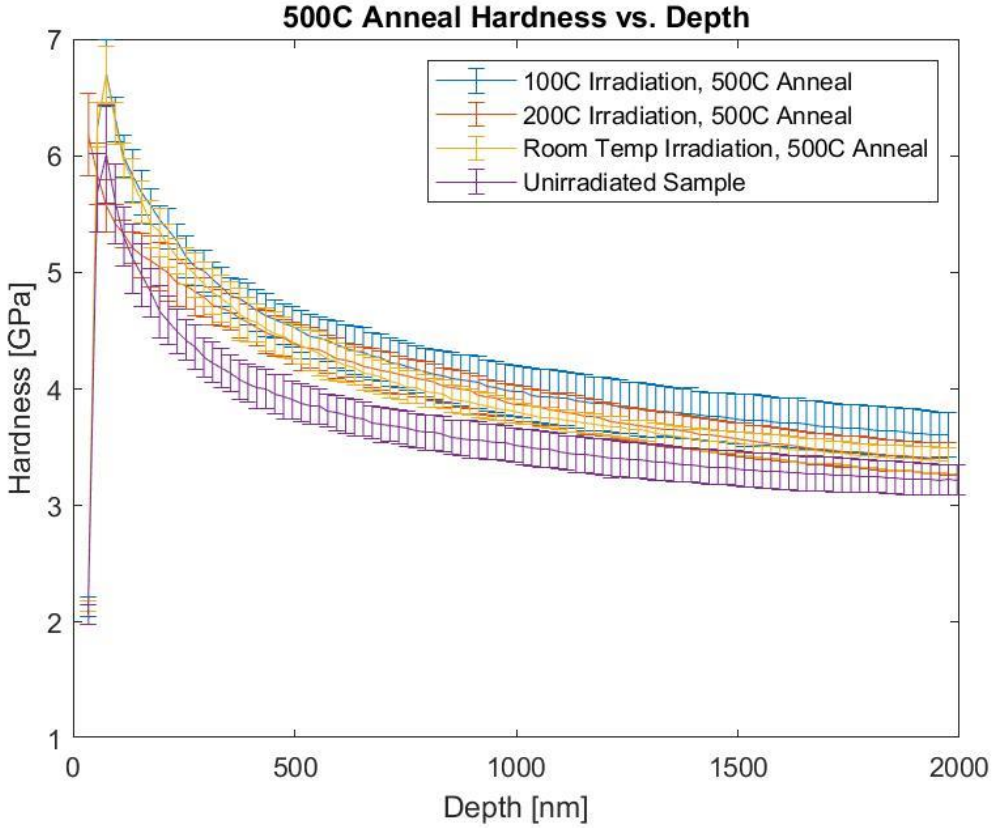

Hardness vs. Depth Curves for 500°C for Several Irradiation Temperatures